

Basis Tensor Decomposition for Restoring Intra-Voxel Structure and Stochastic Walks for Inferring Brain Connectivity in DT-MRI

Alonso Ramirez-Manzanares (alram@cimat.mx) and Mariano Rivera
(mrivera@cimat.mx)

*Centro de Investigacion en Matematicas A.C.,
Apdo. Postal 402, Guanajuato, Gto., 36000, Mexico.*

Abstract. We present a regularized method for solving an inverse problem in Diffusion Tensor Magnetic Resonance Imaging (DT-MRI) data. In the case of brain images, DT-MR imagery technique produces a tensor field that indicates the local orientation of nerve bundles. Now days, the spatial resolution of this technique is limited by the partial volume effect produced in voxels that contain fiber crossings or bifurcations. In this paper, we proposed a method for recovering the intra-voxel information and inferring the brain connectivity. We assume that the observed tensor is a linear combination of a given tensor basis, therefore, the aim of our approach is the computation of the unknown coefficients of this linear combination. By regularizing the problem, we introduce the needed prior information about the piecewise smoothness of nerve bundles orientation. As a result, we recover a multi-tensor field. Moreover, for estimating the nerve bundles trajectory, we propose a method based on stochastic walks of particles through the computed multi-tensor field. The performance of the method is demonstrated by experiments in both synthetic and real data.

Keywords: DT-MRI, DTI, Fiber tractography, Intra-voxel structure, High angular resolution diffusion imaging, Multi-tensor, Stochastic particle walks

1. Introduction

One of the most challenging medical goals is the estimation of brain connectivity in vivo. For this purpose, a special Resonance Magnetic Imaging (MRI) technique named Diffusion Tensor Magnetic Resonance Imaging (DT-MRI) is used. DT-MRI are computed from three-dimensional (3D) Diffusion Tensor Images (DTI). They measure the directional microscopic diffusion of water in tissues, specifically in brain tissue, such a diffusion is constrained by cellular walls. The Stejskal-Tanner equation (Basser et al., 1996; Westin et al., 2002),

$$S_r = S_{0r} \exp(-b\mathbf{g}^T \mathbf{D}_r \mathbf{g}), \quad (1)$$

shows, for a given voxel r , the relationship between the measured signal magnitude without diffusion S_0 , and the one attenuated by the water diffusion in the tissue S . The unitary vector $\mathbf{g} = [g_x, g_y, g_z]^T$ indicates the direction in which a directional independent magnetic gradient is applied, \mathbf{D}_r is a positive definite symmetric tensor that determines an angular diffusion coefficient and b is a constant that depends on the acquisition parameters, see (Westin et al., 2002) for more details. The conventional procedure for computing the tensor field \mathbf{D} is based on a least-squares method with at least 8 diffusion images, $S^{(i)}$:

$$\operatorname{argmin}_{\mathbf{D}_r} \sum_{i=1}^L [\ln S_r^{(i)} - \ln S_{0r} + b\mathbf{g}^{(i)T} \mathbf{D}_r \mathbf{g}^{(i)}]^2, \quad (2)$$

where L is the number of acquired diffusion weighted images, each one corresponding to a magnetic gradient in the $\mathbf{g}^{(i)}$ direction. The least-squares problem (2) is solved for the 6+1 unknowns (Westin et al., 1999). Such unknowns are six independent components of the symmetric diffusion tensor, \mathbf{D}_r , and the diffusion free signal, S_{0r} . One can find in the literature a close-form to fit the diffusion tensor: the tensor \mathbf{D}_r is decomposed in a particular orthonormal tensor basis (Westin and Maier, 2002). However, this method is more sensitive to the pernicious noise effect than the least-squares. Nevertheless the least-squares method,

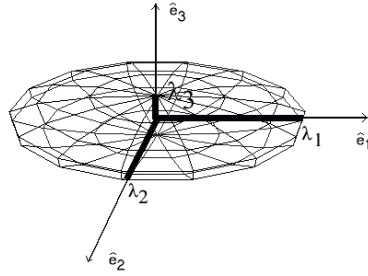


Figure 1. Geometric representation of probability distribution associated to a diffusion tensor.

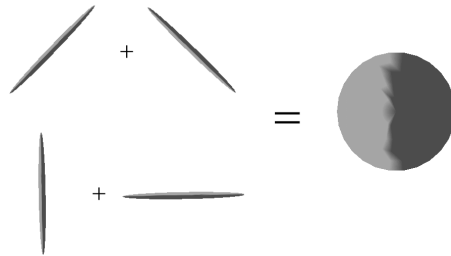


Figure 2. Several combinations of two high-anisotropic tensors produces the same low-anisotropic tensor.

as the method reported in (Westin and Maier, 2002) do not constrain the tensor to be positive definite and a post-processing that guarantees the positiveness is required. For this reason, recently, (Tschumperlé and Deriche, 2003b) and (Wang et al., 2003) proposed regularized methods addressing such a problem.

A diffusion tensor can be visualized as a 3D ellipsoid, as shown in Figure 1. In this geometric interpretation, the principal axis are aligned according to the eigenvectors $[\hat{e}_1, \hat{e}_2, \hat{e}_3]$, the respective eigenvalues, $\lambda_1 \geq \lambda_2 \geq \lambda_3$, define the diffusion magnitude along each axis. Thus, \hat{e}_1 is named the principal diffusion direction (PDD). A study of the behavior of the eigenvalues gives more insight on the angular diffusion variation into the voxels. The relationship between eigenvalues allows one to establish 3 kinds of diffusion (Westin et al., 1999), that corresponds with 3 different levels of anisotropy (anisotropy is a measure of the 3-D asymmetry): a) $\lambda_1 \gg \lambda_2 \simeq \lambda_3$, high anisotropy; the geometric interpretation of such tensor has a cigarette shape, b) $\lambda_1 \simeq \lambda_2 \gg \lambda_3$, medium anisotropy, the

geometric interpretation of the tensor looks like a plate and c) $\lambda_1 \simeq \lambda_2 \simeq \lambda_3$, low anisotropy, this case is visualized as a soccer ball.

In the 3D case, the one concerns here, *fractional anisotropy* (FA) is the most commonly used measure (Basser et al., 1996; Basser et al., 2000):

$$FA(\mathbf{D}) = \sqrt{\frac{(\lambda_1 - \lambda_2)^2 + (\lambda_1 - \lambda_3)^2 + (\lambda_2 - \lambda_3)^2}{2(\lambda_1^2 + \lambda_2^2 + \lambda_3^2)}}, \quad (3)$$

where λ_k is the k^{th} eigenvector of \mathbf{D} . Note that FA is close to one for highly anisotropic tensors, while FA is close to zero for a low anisotropic tensor (the spherical case).

In addition to standard studies on MR images, as the classification of voxels between white/gray matter tissues, the FA of DT-MR images provides tissue information. In white matter, according to medical prior knowledge, one expects high anisotropic coefficients and low anisotropy in grey matter. However, perhaps, the most important information that can be inferred from DT-MR images is tissue connections. That means that, for brain, one could estimate axons bundle pathways by following the PDD's in regions with high anisotropy (sites where FA takes large values). This information is very useful in medical image research, due to the relationship of brain connectivity with several diseases, and in general, with brain development [see (Buxton, 2002; Poldrack, 2001)]. Due to the promissory use of the DT images, now days, one can find works that reports classical computer vision techniques applied to those medical images; for instance segmentation (Zhukov et al., 2003) or nonrigid registration (Ruiz-Alzola et al., 2000; Gee et al., 2002).

As in any other imaging acquisition technique, DT-MR images can be corrupted with noise, and therefore, a filtering processes are required. Other problem concerns the limited resolution for dealing with partial volume voxels. This is, when a voxel contains a cross or a bifurcation of fibers. In the following subsection we discuss the problem produced by this partial volume effect.

1.1. STATEMENT OF THE PROBLEM

Noise is not the only problem precluding DT–MR images; partial volume voxels have a more pernicious effect than in standard MR images: the observed diffusion tensor at voxels where two or more fibers cross, split or merge, is the addition of several diffusion tensors,—each one aligned with a particular bundle fiber. The addition of two almost orthogonal tensors with high–anisotropy results in a tensor with low–anisotropy. This fact increases the uncertainty of the tissue orientation (the inverse problem is not well–defined, see figure 2)(Westin et al., 2002; Wiegell et al., 2000). So, one needs to solve these issues in order to recover the two tensors that produced the measured one.

If the image spatial resolution is increased, then the partial volume effect can be reduced in voxels located at boundaries of differently oriented tissues, but with a significant increment of the acquisition time. However, the partial volume effect produced by fiber crossing can not be diminished by increasing the spatial resolution. Therefore, in order to compute a good estimation of the original fiber pathways, it is necessary to develop a process that recover the lost intra–voxel information.

There are several methods reported in the literature for estimating fiber pathways. Those methods are based on: performing deterministic walks of particles on the tensor field by following the PDD, partial differential equations (Basser et al., 2000; Basser et al., 2002), local regularization techniques (Poupon et al., 2000; Zhukov and Barr, 2002), or the propagation of a wavefront by using a fast marching method (Parker et al., 2002). In (Björnemo and Anders, 2002), the displacement direction of a particle is computed with a deterministic method. Then, this direction is randomly disturbed in order to introduce a stochastic behavior. (Lazar et al., 2003) proposed a method called TEND (TENSor Deflection), that produces smooth fiber trajectories by enforcing the new particle direction to be close to the previous direction and the tensor PDD in the current

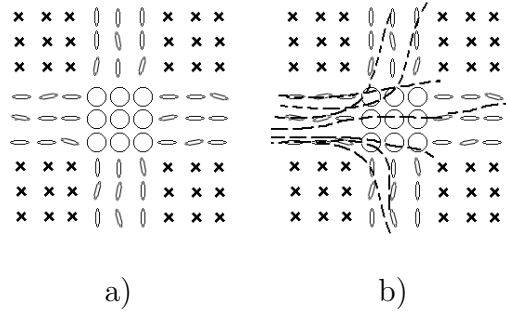


Figure 3. a) Schema of a tensor field on a fiber crossing. b) particles walking through the horizontal fiber path; most particles are deviated from the right trajectory, due to the uncertain direction on the cross.

position. The compromise between these two lead directions is weighted by the local FA coefficient. In any case, the partial volume effect reduces the estimated fiber pathways accuracy.

Figure 3 illustrates the estimation of fiber pathways in a fiber crossing. As one can see, the intersection of two bundle fibers produces a region where the local orientation is uncertain ($FA \simeq 0$). In order to ensure that the particles chose the right trajectory through the fiber crossing, they should reach to the low confident region with a trajectory aligned to the tracked fiber. Otherwise, the particle trajectory could be bent. To achieve this, in (Westin et al., 2002; Westin et al., 1999; Björnemo and Anders, 2002) is applied an homogeneous Gaussian smoothing to the tensor field. Although the blurring produces a denoising effect, it also increases the orientation uncertainty. The approach reported in (Zhukov and Barr, 2002) aims to reduce such uncertainty by computing the displacement of each particle with a direction computed with a robust anisotropic average of the tensors in a neighborhood surrounding the particle. One can also find regularized schemes for fiber tractography: (Tschumperlé and Deriche, 2002) proposed a regularized filter for orthonormal vector fields, as the defined by the eigen-vector field of DT images. However, the lost intra-voxel structure is not revealed. In their seminar work (Poupon et al., 2000) proposed a Bayesian regularized based method. In such a work, the moving direction is deterministically

computed as a MAP estimator that combines the PDD (at the current voxel) and the a smooth extrapolation of the past trajectory.

The partial volume effect in DT-MR has capture the attention of recent research. This is the case of the Tuch et al. work (Tuch et al., 1999; Tuch et al., 2002; Tuch, 2002). They proposed a high angular resolution imaging method based on an observation model built by a finite mixture of Gaussians:

$$S_i = S_0 \sum_{j=1}^M \beta_j \exp(-bg_i^T R_j^T \Lambda R_j g_i), \quad (4)$$

where Λ is a fixed diagonal matrix of positive eigen-values. The unknowns, in (4), are: the β coefficients, the rotation angles in R and the number M of Gaussians. Such unknowns must be computed, independently for each voxel from a large set of acquired images $\{S\}$. This Diffusion Multi-Tensor Magnetic Resonance Imaging (DMT-MRI) technique allows one to recover the intra-voxel information that is not observed in the standard DT-MRI. The drawbacks of the method are: the large number of additional diffusion images $\{S\}$ required (for instance, in (Tuch, 2002) are used 126 diffusion 3D-images), the consequent increment on their acquisition time and the algorithmic problems related to Equation (4), which is highly nonlinear. So that, multiple restarts of the optimization method are required to prevent the algorithm from settling in a local minima. Furthermore, no stable solution has been reported for more than 2 fiber bundles, i.e. for $M > 2$ [see discussion in Ref. (Tuch, 2002), Chap. 7].

Visualization of fibers is other topic of recent research: streamtubes and streamsurfaces (Zhang et al., 2000), the creation of textured representations of dense tensor-valued fields (Tschumperlé and Deriche, 2003a) and measures maps of brain connectivity (O'Donnell et al., 2002). In this paper we do not deal with the visualization problem and our visualization tools are intuitive and basic.

It is well known the limitation of DT-MRI for representing the intra-voxel geometric/structure of multi-modal water diffusions. So that, techniques that di-

rectly uses raw data [$S^{(i)}$ in (2)] have recently been proposed. Such techniques are named High-Angular Resolution. In our knowledge, the here proposed method is the first one in reconstructing the intra-voxel structure from DT-MR images. This allows to medical researchers to reuse the existing DT-MR databases and perform new studies, that in other way could not be done. Actually, the paper (Ramirez-Manzanares et al., 2004) presents the extension of the here proposed method for working directly with raw data.

The method we propose here, based on a preliminary version introduced in (Ramirez-Manzanares and Rivera, 2003), consist of two stages: i) restoration of the intra-voxel information by computing the coefficients of a tensor basis field and ii) estimation of fiber pathways by particle stochastic walks. The method for reconstructing the intra-voxel information uses standard DT-MR images as input data. That means that existing large data base or new measurements of DT-MR images can be processed at a fraction of the acquisition time with respect to DMT-MR images. Additionally, the proposed method is based on the minimization of a cost function based on quadratic potentials. Such minimization can efficiently be performed with standard deterministic algorithms, in particular, we used an iterated Gauss-Seidel scheme. In the second stage, we estimate bundle fibers with a stochastic walk procedure formulated in a Bayesian framework. This particles walk method is close related with (Poupon et al., 2000) formulation. Differently, in our case there are several possible PDD's in a voxel and the posterior distribution of the moving directions is multi-modal. Therefore, the new position of the particle is computed by sampling the posterior distribution of the displacement directions. In order to compute this posterior distribution, we take into account: the information of the reconstructed diffusion multi-tensor field in a likelihood term and the last positions of the particle in a prior term (regularization). The prior term promotes smooth trajectories.

The structure of this paper is as follows. Section 2 presents the proposed restoration method for the intra-voxel structure information. Section 3 presents

the stochastic walk method for estimating the axon bundle pathways. Section 4 describes experiments with both synthetic and real DT–MR images and a validation procedure for the recovered data and, finally, section 5 presents our conclusions.

2. Restoration of Intra–Voxel Information

This section introduces the first stage of the method: the procedure for recovering the intra–voxel structure. In order to motivate our approach, we first present the observation model of the measured diffusion tensor field.

2.1. OBSERVATION MODEL OF THE DIFFUSION TENSOR

Differently to the method reported in (Tuch et al., 1999; Tuch, 2002; Ramirez-Manzanares et al., 2004) [eqn. (4)], we suppose that the raw data set $\{S\}$ is not accessible, but the measured (fitted) tensor field \mathbf{D} . However, in the above referenced works is established the model, for two diffusion directions based on the mixture of two Gaussians: $S^{(i)}/S_0 = \exp(-bg_i^T \mathbf{T}_1 g_i) + \exp(-bg_i^T \mathbf{T}_2 g_i)$; therein is noted that for small b -values one has that: $S^{(i)}/S_0 \approx \exp(-bg_i^T (\mathbf{T}_1 + \mathbf{T}_2) g_i) = \exp(-bg_i^T \mathbf{D} g_i)$ with the observed tensor $\mathbf{D} = \mathbf{T}_1 + \mathbf{T}_2$. Therefore, we assume that \mathbf{D} is the summation of individual tensors \mathbf{T}_i :

$$\mathbf{D}_r = \sum_i^{M_r} \mathbf{T}_{ir} + \eta_r; \quad (5)$$

where M_r is equal to the number of fibers with a different orientation (note that M depends on the voxel), and η is a small residual tensor produced by noise. Such former tensors, \mathbf{T}_{ir} , correspond with no–collinear fibers into the voxel, r . The solution of the inverse problem implicit in (5), involves the computation of the tensors $\{\mathbf{T}_{ir}\}$, with arbitrary size and orientation and their number M_r . For

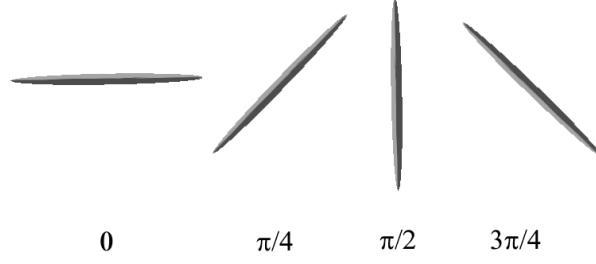


Figure 4. A example of 2D tensor base set $\bar{\mathbf{T}}$, with cardinality equal to four.

that reason, instead of the “exact” model (5), we propose to use an approximated model based on a predefined tensor basis, $\bar{\mathbf{T}}$. These base tensors are chosen such that they are uniformly distributed on the 3D space of orientations, and they have $\text{FA}(\bar{\mathbf{T}}_i) \approx 1$ (Figure 4 shows a 2D example of a basis set of four tensors with their orientations uniformly distributed in the interval $[0, 2\pi]$). Therefore, the approximated observation model is [compare with (4) and (5)]:

$$\mathbf{D}_r = \sum_i^N \alpha_{ir} \bar{\mathbf{T}}_i + \bar{\eta}_r, \quad (6)$$

where N is the cardinality of the base $\bar{\mathbf{T}} = [\bar{\mathbf{T}}_1, \bar{\mathbf{T}}_2, \dots, \bar{\mathbf{T}}_i, \dots, \bar{\mathbf{T}}_N]$ and $\alpha = [\alpha_1, \alpha_2, \dots, \alpha_i, \dots, \alpha_N]^T$ is a vector field, such that the positive scalar α_{ir} denotes the contribution, at the voxel r , of the base tensor $\bar{\mathbf{T}}_i$ to the observed tensor, \mathbf{D}_r . Note that the basis $\bar{\mathbf{T}}$ is, in general, not complete. For instance, a tensor $\mathbf{D} = \mathbf{v}\mathbf{v}^T$ (with $\mathbf{v} = [\cos \pi/8, \sin \pi/8]$) is not a linear combination of the basis tensor in Figure 4. Therefore, the new residual, $\bar{\eta}_r$, is produced by noise and by the limited angular resolution of the basis, $\bar{\mathbf{T}}$. However, if one uses a tensor basis with high angular resolution (N relatively large), one can expect that in a voxel where there is only one fiber path, a single coefficient α_i will take a significant large value and the others $\alpha_{j \neq i}$ would take values close to zero and, as a consequence, one has $\bar{\eta}_r \approx \eta_r$ [see (5)]. In the same way, if there are m different fiber paths in a voxel, then we expect that m coefficients α_k will take a significant large value with respect to the other coefficients.

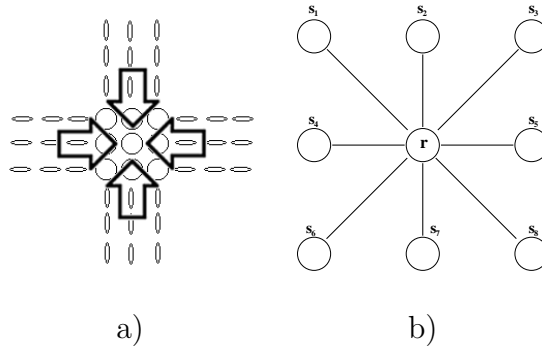


Figure 5. a) Information propagation from the anisotropic to isotropic regions. b) A 2D second order neighborhood \mathcal{N}_r of the voxel r .

2.2. COST FUNCTION FOR RESTORING INTRA-VOXEL DT-MRI STRUCTURE

Model (6) can represent more than one tensor in a voxel, but, it is still necessary to determine which linear combination of base tensors, in $\bar{\mathbf{T}}$, best fit the data \mathbf{D}_r . Unfortunately, the computation of the positive coefficients, $\{\alpha_{ir}\}$, is an ill-posed problem because the information provided by the observed tensor, \mathbf{D}_r , and the model (6) is not enough for computing a unique solution. So that, we regularize the problem by using the voxel spatial context information. Thus, we want to propagate the coefficient information, in white matter segmented tissue, from regions with high anisotropy to those with low anisotropy. This is consistent with prior knowledge that fiber crossing occurs in regions with low anisotropy, as it is illustrated in Figure 5a. To solve this problem, we propose to minimize a cost function of the form:

$$\hat{U}(\alpha) = \sum_r U(\alpha; r). \quad (7)$$

This global cost \hat{U} is the summation of the individuals cost functions $U(\alpha; r)$ associated to each voxel, r . A preliminary version of the local cost function is:

$$U(\alpha; r) = \rho_1 \left(\sum_i \alpha_{ir} \bar{\mathbf{T}}_i, \mathbf{D}_r \right) + \lambda_s \omega_r \sum_{s \in \mathcal{N}_r} \rho_2(\alpha_r, \alpha_s) + \lambda_c \rho_3(\alpha_r), \quad (8)$$

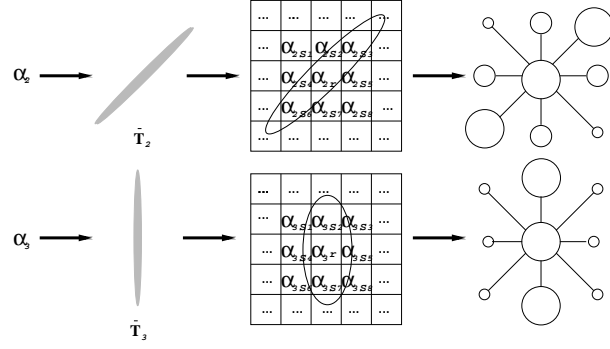


Figure 6. Anisotropic filtering for each layer α_i , in the orientation of the associated base tensor $\bar{\mathbf{T}}_i$, and the schema of the anisotropic filter kernel generated.

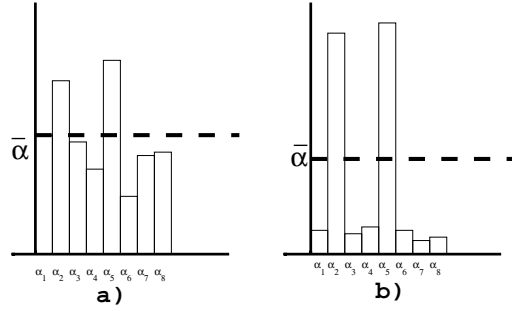


Figure 7. a) Coefficients with low contrast: high uncertainty about the significance of the basis tensors. b) High contrasted coefficients: low uncertainty (see text).

where, in general, the potential functions ρ_j (with $i = 1, 2, 3$) define norms. In next paragraphs, we clarify the meaning of each term in (8).

The first term corresponds to the negative log-likelihood in the Bayesian regularization framework (Geman and Geman, 1984; Li, 2001). This term penalizes the difference between the proposed model and the observed tensor, \mathbf{D}_r . In this particular case, we use the Frobenius's norm for quantifying such a difference. Then $\rho_1(\sum_i \alpha_{ir} \bar{\mathbf{T}}_i, \mathbf{D}_r) = \|\sum_i \alpha_{ir} \bar{\mathbf{T}}_i - \mathbf{D}_r\|_F^2$. Appendix A shows the residual model that lead us to the Frobenius's norm as the negative log-likelihood.

The second term (first regularization term) codifies the prior knowledge by penalizing the spatial inhomogeneity of the vector α . In order to promote the propagation of coefficients information from the regions with high anisotropy to those regions with low anisotropy, and to restrict the opposite (see figure 5a), we weigh this regularization term with the inverse of *fractional anisotropy* of the

data: $\omega_r = 1/FA(\mathbf{D}_r)$, see Eq. (3). The relative contribution of this term, to the total cost, is controlled by the parameter λ_s . \mathcal{N}_r is the set of the 3D first neighbors voxels of r (a second order neighborhood system), see Figure 5b. Additionally, we want to constraint this smoothness process to be performed along the fiber bundle. This is achieved by an anisotropic filtering of the coefficients α . Therefore, we use the tensor $\bar{\mathbf{T}}_i$ as the inertia tensor for controlling such anisotropic filtering of the layer α_i , see Figure 6. Thus, ρ_2 is a weighted quadratic potential of the first differences: $\alpha_r - \alpha_s$. (Viguera, 2001) proposed a method for compute these weights given an inertia tensor $\bar{\mathbf{T}}_{ir}$: $w_{irs} = (s - r)^T \bar{\mathbf{T}}_{ir} (s - r) / \|s - r\|^4$, where w_{irs} is the weight associated with the potential: $(\alpha_{ir} - \alpha_{is})^2$.

Finally, the third term, controlled by the parameter λ_c , promotes large contrast in the α_{ir} coefficients. Figure 7a shows a low contrast example, with high uncertainty about discerning which tensors are more representative. On the other hand, Figure 7b shows an example with low uncertainty: only two coefficients have large values and the others are close to zero. The analysis of Figure 7 deal us to the method for improving the contrast i.e.: by forcing each α_{ir} coefficient to be different from their arithmetic mean: $\bar{\alpha}_r = \sum_i \alpha_{ir}/N$.

Already we have all the ingredients for the final local cost function:

$$U(\alpha, r) = \sum_j \left(\sum_i \alpha_{ir} \bar{T}_{ij} - D_{rj} \right)^2 + \lambda_s \omega_r \sum_{s:s \in \mathcal{N}_r} \sum_i w_{irs} (\alpha_{ir} - \alpha_{is})^2 - \lambda_c \sum_i (\alpha_{ir} - \bar{\alpha}_r)^2; \quad (9)$$

with the additional constraint $\alpha_{ir} \geq 0, \forall i$, where $i = 1, \dots, N$ and $j = 1, 2, \dots, 9$ is an index that runs over the tensor (a 3×3 matrix) coefficients.

2.3. MINIMIZATION ALGORITHM

The minimization of Eq. (7) is achieved by solving the linear system [(9) is quadratic] that results from $\nabla \hat{U}(\alpha) = 0$ and with $\alpha \geq 0$. We use a simple Gauss-

Seidel scheme, with the additional advantage of low memory requirements, for solving this linear system. Such iteration is:

$$\alpha_{kr}^{t+1} = \frac{-\sum_j \left(\sum_{i \neq k}^N \alpha_{ir}^t \bar{T}_{ij} - D_{jr} \right) \bar{T}_{kj} + \lambda_s \omega_r \sum_{s: s \in \mathcal{N}_r} w_{krs} \alpha_{ks}^t - \lambda_c C_1 \sum_{i \neq k}^N \alpha_{ir}^t}{\sum_j \bar{T}_{kj} + \lambda_s \omega_r \sum_{s: s \in \mathcal{N}_r} w_{krs} + \lambda_c C_2}, \quad (10)$$

where $C_1 = Z_A - Z_A^2 Z_C + Z_A Z_B$ and $C_2 = Z_A Z_B - Z_A^2 Z_C - Z_B$, with $Z_A = 1/N$, $Z_B = 1 - Z_A$, $Z_C = N - 1$.

The non-negativity constraint on α_{ir} is satisfied by projecting to zero the negative values at each α_{kr}^{t+1} computation in (10). Following the Gauss-Seidel minimization scheme, it is necessary to perform a few iterations over the N α -coefficients at the r position before to update the next position, $r + 1$. Note that, if the contrast term is turn off ($\lambda_c = 0$); Eq. (9) is a quadratic programming problem and a global minima can be computed. However, in the case of $\lambda_c > 0$, the cost function could be no-convex and many local minima are possible. For this reason is applied a continuation strategy for the parameter λ_c : we initially set $\lambda_c = 0$, and then, once the algorithm has converged (with a low contrast on the α_r vectors), the right value of λ_c is used for refining the solution.

3. Stochastic Walks for Estimating Fiber Pathways

The second stage of the method for recovering fiber pathways in DT-MRI, is the computation of virtual particles walks through the multi-tensor field. In opposition to deterministic walk methods, reported in (Basser et al., 2000; Poupon et al., 2000; Zhukov and Barr, 2002), our approach consist of stochastic walks.

Before to present the stochastic walk method, we establish some definitions. \mathbf{x}_t denotes the position vector of a particle at iteration t , d_{t+1}^* is the direction (unitary vector) that leads the particle from the position \mathbf{x}_t to the next step,

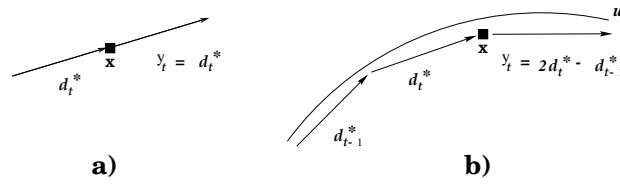


Figure 8. Definition of \mathbf{y}_t for a) the first order walk and b) second order walk.

\mathbf{x}_{t+1} , and δ is the step size, i.e. $\delta = |\mathbf{x}_{t+1} - \mathbf{x}_t|$, then:

$$\mathbf{x}_{t+1} = \mathbf{x}_t + \delta d_{t+1}^*. \quad (11)$$

In our case, the particles pathways are close related with the fiber structure. Therefore, we use the basis tensor decomposition introduced in section 2 in order to infer the fiber pathways. Thus, the basis tensor decomposition coefficients control the stochastic walks of the virtual particles. One can expect that in voxels where only one fiber is present, a single coefficient of the tensor basis field has a significant large value and its PDD indicates the fiber orientation. On the other hand, in a bifurcation two coefficients have significant values. The particle should choose any of those paths corresponding to the PDD's.

In the simple case of one predominant displacement orientation, μ (note that the PDD is associated with both \hat{e}_1 and $-\hat{e}_1$), we modeled the likelihood of a new position of a particle, given the predominant orientation and the last position, with the Dimroth–Watson distribution (Mardia, 1972):

$$P(\mathbf{x}_{t+1} | \mathbf{x}_t, \mu) = \frac{1}{K} \exp\left(\kappa \left[\mu^T \frac{(\mathbf{x}_{t+1} - \mathbf{x}_t)}{\delta}\right]^2\right) = \frac{1}{K} \exp(\kappa |\mu^T d_{t+1}^*|^2); \quad (12)$$

where the parameter, κ , regulates the concentration around $\pm\mu$, and K is a normalization constant.

In the next subsection we discuss how the direction d_{t+1}^* and the step size δ are chosen based on the tensor basis decomposition, i.e., we expand the model given by equation (12) for the case with several PDD's per voxel.

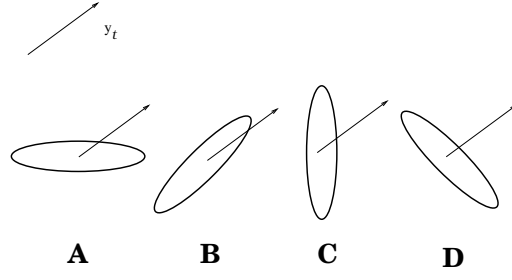


Figure 9. Calculation of the term $P(d_{t+1} \parallel q_i \mid \{d_t^*\})$.

3.1. COMPUTATION OF THE DISPLACEMENT DIRECTION

For computing the displacement direction, d_{t+1}^* in (11), we use a Bayesian estimation principle based on Markov processes, as it is following explained. Let $\mathbf{q} = \{q_1, q_2, \dots, q_N\}$ a set of unitary orientation vectors (q_i and $-q_i$ are not distinguished) each one aligned with the corresponding PDD's of the base tensors, $\bar{\mathbf{T}}$. Then, by using the Bayes Rule, we compute the probability of choosing a particular q_i orientation, as the orientation of the vector d_{t+1} , given the α -coefficient vector at the position r and the sequence of previous displacements: $d_1^*, d_2^*, \dots, d_t^*$, denoted by $\{d_t^*\}$, with¹ :

$$P(d_{t+1} \parallel q_i \mid \alpha_r, \{d_t^*\}) = \frac{1}{Z} P(\alpha_r \mid d_{t+1} \parallel q_i, \{d_t^*\}) P(d_{t+1} \parallel q_i \mid \{d_t^*\}), \quad (13)$$

where Z is a normalization constant, and $x \parallel y$ denotes that x is parallel to y . The vector d_{t+1}^* is computed by performing a sampling of the posterior probability distribution (13). This process can be understood as a stochastic tournament. The ambiguity in the sign of the orientation is solved by choosing from d_{t+1} and $-d_{t+1}$, the one with positive inner product with the extrapolated past direction, i.e. the closest direction with the past trajectory.

The first term in (13), likelihood term, can be simplified by using the independence between the coefficients α , at the current position, and the sequence

¹ Due that: $P(A|B, C) = P(B|A, C) P(A|C) / P(B|C)$

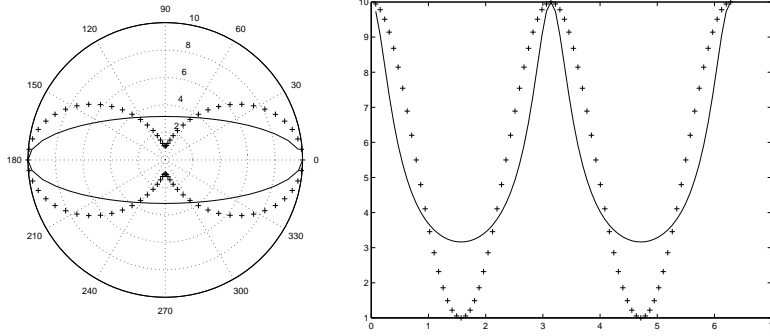


Figure 10. Functions for prior probability distributions: $\exp(-\mathbf{y}_t^T \bar{\mathbf{T}}_i \mathbf{y}_t)$ [in (+)] and $1/\sqrt{\mathbf{y}_t^T \hat{\mathbf{T}}_i \mathbf{y}_t}$ (in continue line). Polar (left) and rectangular (right) plots.

$\{d_t^*\}$:

$$P\left(\alpha_r \mid d_{t+1} \parallel q_i, \{d_t^*\}\right) = P\left(\alpha_r \mid d_{t+1} \parallel q_i\right). \quad (14)$$

We model this distribution with a probability mixture model of the form (Hastie et al., 2001) [compare with (12)]:

$$P\left(\alpha_r \mid d_{t+1} \parallel q_i\right) = \frac{1}{Z_M} \sum_j^N \beta_{rj} \exp(\kappa(q_i^T q_j)^2), \quad (15)$$

where the mixing proportion parameters β_{rj} are computed by normalizing the α_{rj} coefficients, i.e.

$$\beta_{rj} = \frac{\alpha_{rj}}{\sum_k \alpha_{rk}}, \quad (16)$$

this satisfy $\sum_j^N \beta_{rj} = 1$. Given that the particle positions are real valued ($\mathbf{x}_t \in \Omega \subset \mathbb{R}^3$), then, mixture coefficients β_{x_t} are computed with a trilinear interpolation. Note that for a very large value of the κ parameter, one obtains sharper distributions [i.e. $\exp(\kappa(q_i^T q_j)^2) = 1$ if $i = j$ and it is equal to zero otherwise]. In such case the computation of the likelihood is simplified:

$$P\left(\alpha_r \mid d_{t+1} \parallel q_i\right) = \beta_{x_t i}. \quad (17)$$

This reduce significantly the computational time, specially for a large numbers of particles and displacement steps.

The prior probability in (13) codifies our prior knowledge about smooth fiber trajectories. Specifically, this prior promotes that d_{t+1}^* extends the sequence $\{d_t^*\}$ in a smooth way. If the stochastic walk is modelled as a Markovian process, then the smoothness constraint, on d_{t+1}^* , depends on a few past steps. For instance, we define the unitary vector: $\mathbf{y}_t = d_t^*/|d_t^*|$ for a first order Markov processes that preserves the last tendency, or

$$\mathbf{y}_t = (2d_t^* - d_t^*)/|2d_t^* - d_t^*| \quad (18)$$

for a second order Markov processes that preserves the last curvature, see Figure 8. Then, we use

$$P\left(d_{t+1} \parallel q_i \mid \{d_t^*\}\right) = \frac{1}{Z_2} \frac{1}{\sqrt{\mathbf{y}_t^T \hat{\mathbf{T}}_i \mathbf{y}_t}} \quad (19)$$

as prior probability for $d_{t+1} \parallel q_i$; where Z_2 is a normalization constant, $\hat{\mathbf{T}}_i = \text{trace}[\bar{\mathbf{T}}_i] \mathbf{I} - \bar{\mathbf{T}}_i$ is the inertia tensor associated to the i^{th} base tensor, $\bar{\mathbf{T}}_i$. A geometric interpretation shows that (19) corresponds to the radius, ρ , in the \mathbf{y} -direction of the 3D-ellipsoid defined by the level set: $(\rho \mathbf{y}_t)^T \hat{\mathbf{T}}_i (\rho \mathbf{y}_t) = Z_2$. This is illustrated by Figure 9; the radius in the direction \mathbf{y}_t is measured for the base tensors corresponding to Figure 4. In this way, it is clear that the largest value is computed with the tensor B. Consequently, in this case, it is more probably than the next walk direction is parallel to the PDD of the base tensor B. We use (19) instead of, the apparently natural Bingham's distribution (Mardia, 1972):

$$P\left(d_{t+1} \parallel q_i \mid \{d_t^*\}\right) \propto \exp(-\mathbf{y}_t^T \bar{\mathbf{T}}_i \mathbf{y}_t), \quad (20)$$

because (19) is sharper for high probabilities and allows us a clearer distinction between close orientations, see Figure 10.

3.2. IMPLEMENTATION DETAILS

Given that the computed walk have coarse trajectories because of the discrete nature of the tensor basis, we refine the vector d_{t+1}^* in order to obtain smooth

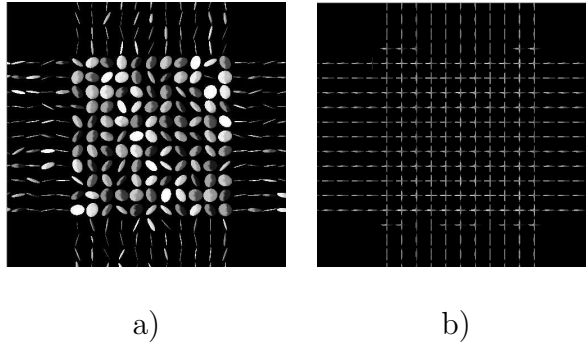


Figure 11. A 2D synthetic fiber crossing. a) The data tensor field. b) The 2D recovered multi-tensor field.

trajectories. Such refinement consists on to use as displacement vector the resultant sum of two vectors: the previous direction step d_t^* , and the winner of the stochastic tournament, d_{t+1}^* . Note that, the refined orientation does not necessary belongs to the set \mathbf{q} .

4. Experiments

In this section, we demonstrate the performance of the method by numerical experiments in both synthetic and real DT-MR data. In the second subsection we show the validation of the obtained results. All the stochastic walks were performed using the second order Markov process model, (18).

4.1. RESULTS

Figure 11 shows the results of the first experiment in synthetic two-dimensional (2D) data. Panel 11a shows the noisy tensor field with a fiber crossing. The restored multi-tensor field is shown in panel 11b. Note that, the correct two base tensors are recovered at the intersection and the noise is practically filtered. Thus, the method discover the intra-voxel structure. Only the base tensors with the α_i coefficients that represent at least the 95% of the linear combination are

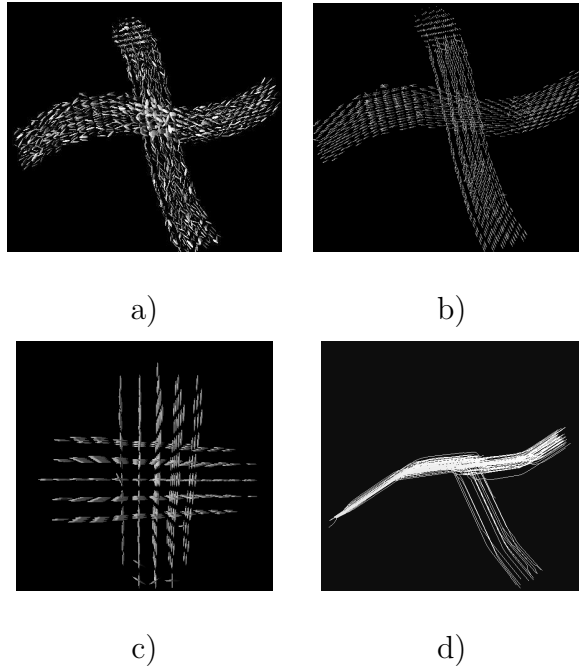


Figure 12. Results of the numerical experiment with synthetic data (see text).

displayed. The parameters of the method were $N = 6$, $\lambda_s = 1.0$, $\lambda_c = 0.1$. We choose the base tensors such that their eigen-values are $[\lambda_1, \lambda_2] = [1, 0.1]$.

The second experiment was performed on the 3D synthetic data shown in Figure 12, panel (a). In this case, the tensors show smooth wavy paths with no orthogonal intersection. Panels 12b and 12c show the recovered multi-tensor field and the detail of the intersection, respectively. Panel 12d shows the particle paths of a set of 100 particles with starting point in the left part of the horizontal fiber. We note that approximately the 15% of the particles are deviated to the other simulated fiber bundle. This feature is product of the stochastic nature of the particle walks and allows us to explore possible bifurcations in fiber bundles. In comparison, deterministic walk methods will recover the same trajectory for all the particles that were started at the same point. The parameters of the method are: 33 orientations (N) that sample uniformly the 3D orientation space, $\lambda_s = 0.07$, and $\lambda_c = 0.05$. The image test dimensions are $32 \times 32 \times 32$ voxels. In this case, we choose the base tensors, such that their eigen-values are

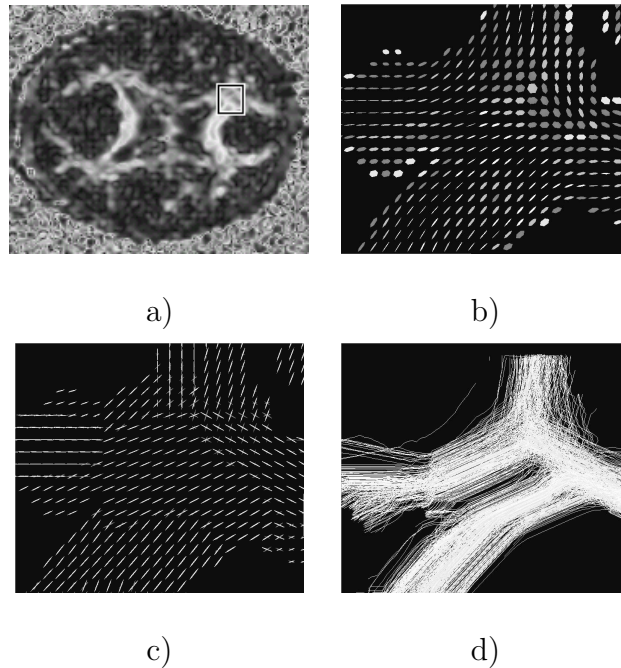


Figure 13. Results of the numerical experiment with standard DT-MRI data (see text).

$[\lambda_1, \lambda_2, \lambda_3] = [1, 0.1, 0.1]$. We select this tensor basis based on the *prior* knowledge that diffusion along the fiber PDD is about 10 times larger than the diffusion in the transversal directions of real axon fibers (Buxton, 2002).

Figures 13 and 14 show the results of an experiment with real DT-MRI data. The original DT-MRI data were acquired with a resolution of $128 \times 128 \times 20$, and each voxel corresponds to a volumetric space of $2mm \times 2mm \times 4mm$. We interpolate the data, so that, each interpolated voxel have a dimension of $1mm \times 1mm \times 1mm$ (it corresponds to $186 \times 154 \times 60$ voxels in the region of interest, i.e. the parallelogram that contains brain tissue). The interpolation was performed by using the DT data approximation method reported in (Pajevic et al., 2002), with a scaling factor $\Delta = 0.5$. Panel 13a shows the *fractional anisotropy* of an axial slice of the interpolated data (used as input to the algorithm for recovering the intra-voxel structure) and the small square indicate the region of detail. Panel 13b shows the region of detail of the interpolated DT. Panel 13c shows, the detail of the recovered multi-tensor field and Panel 13d the computed trajectories



Figure 14. particle trajectories computed with the stochastic walk in the recovered multi-tensor field.

of the particles. In this case, the displacement of the particles was constrained to lay in the axial slice shown in Panel 13a. Figure 14 shows the full view of several pathways computed in the mentioned slice. It is important to note that the set of parameters and the tensor basis were the same used in the experiment of Figure 12.

Finally, figure 15 shows the result of the experiment designed to demonstrate the capability of the method for filtering tensor fields. Panel 15a shows a region of DT-MRI input data, panel 15b shows the recovered multi-tensor field and panel 15c shows the reconstructed tensor field \mathbf{D}_r^f . Such reconstruction is computed with [see the direct model (6)]:

$$\mathbf{D}_r^f = \sum_i^N \alpha_{ir} \bar{\mathbf{T}}_i. \quad (21)$$

Note that the restored tensor field is congruent with the input data and the enhancement is evident: the restoration have more defined local orientations and a higher anisotropy.

The last experiment with real data was performed in order to study a section of the corona radiata in a human brain. Figure 16 shows the results with a crossing fiber region. The recovered intra-voxel structure is congruent with the

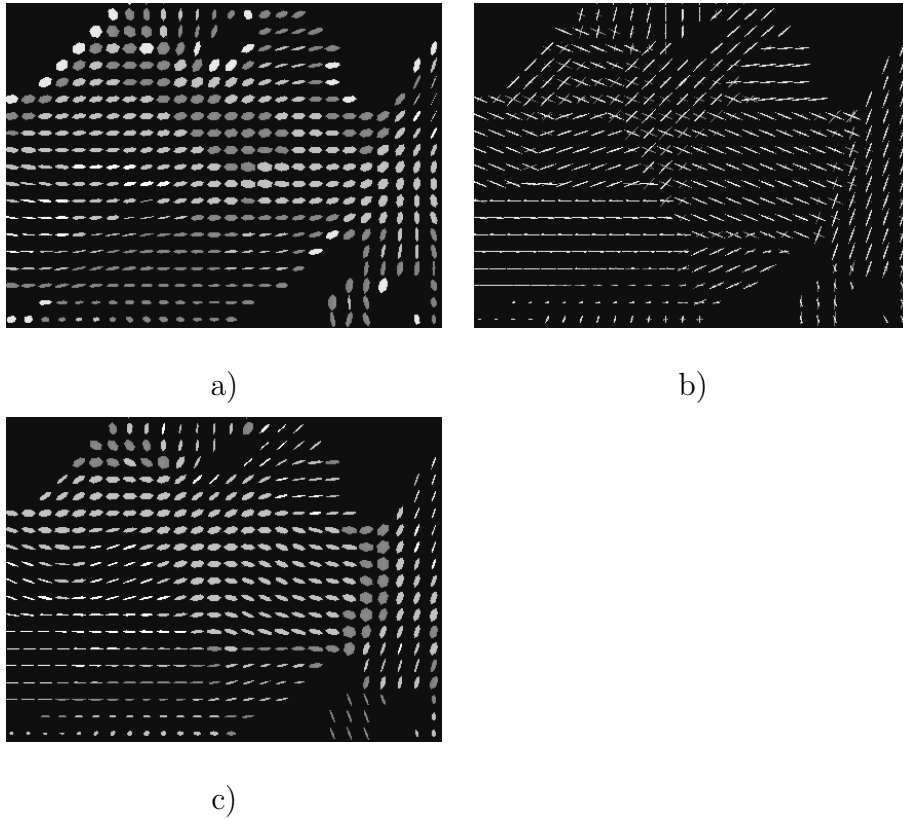


Figure 15. Filtering of tensor fields (a region of detail). a) DT-MRI input data. b) intra-voxel restoration and c) filtered tensor field (see text).

a priori anatomical knowledge for that region, see (Poupon et al., 2000, Figure 3).

4.2. RESULTS VALIDATION

The validation procedure consist in to generate synthetic diffusion tensors corresponding to a two wavy fibers crossing. For each voxel, we established, for each fiber, the diffusion coefficients D and the orientation present.

Then, we compute the S_i , ($i = 1, \dots, 4$) signal decay coefficients according with the expression in (Buxton, 2002, Chapter 9):

$$S_i = S_0 \exp [-b(D_1 \cos^2 \theta_i + D_2 \sin^2 \theta_i)] \quad (22)$$

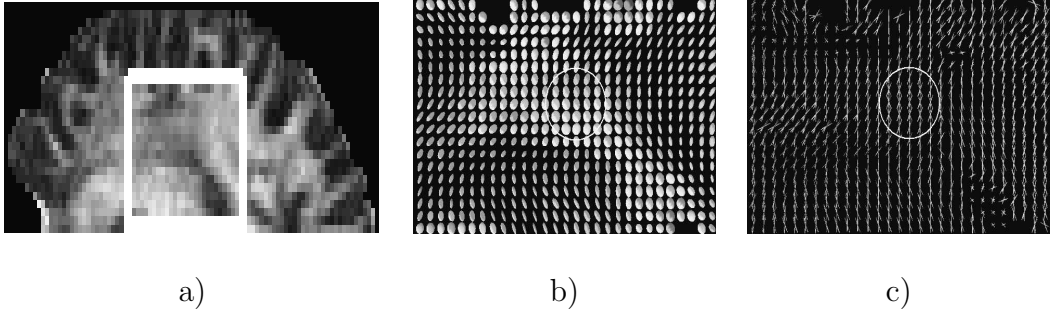


Figure 16. Results for a corona radiata section. a) FA map, the region of interest (ROI) is marked, b) standard DT field of the ROI, the circle shows a crossing zone, and c) the multi-tensor field recovered, see text.

in the case of one fiber present in the voxel, or

$$S_i = S_0 \exp [-b(D_1 \cos^2 \theta_i + D_2 \sin^2 \theta_i + D_3 \cos^2 \phi_i + D_4 \sin^2 \phi_i)] \quad (23)$$

if there are two; where D_1, D_2 are the principal and secondary diffusion coefficients of the first fiber and D_3, D_4 are the principal and secondary diffusion coefficients of the second fiber ($\frac{D_1}{10} \approx \frac{D_3}{10} \approx D_2 \approx D_4$), θ_i and ϕ_i are the angles between the orientation of the principal diffusion for the first and second fiber respectively with the i -th acquisition axis (see figure 17). The b coefficient was set to 1000 s/mm^2 according to the standard DT-MRI protocol, and $D_1 = 1 \times 10^{-3} \text{ mm}^2/\text{s}$ (typical for brain white tissue). Once the signal decay coefficients, S_i , were generated, we fitted the tensor with the Least-Square method reported in (Westin et al., 1999).

The last step in the validation procedure is to obtain the multi-tensor field accord to the method described in section 2.

We measured the difference between :

1. The original diffusion orientations and the recovered multi-tensors PDD's.
2. The trace of the original tensor and the trace of the addition of the recovered multi-tensors [see equation (21)].

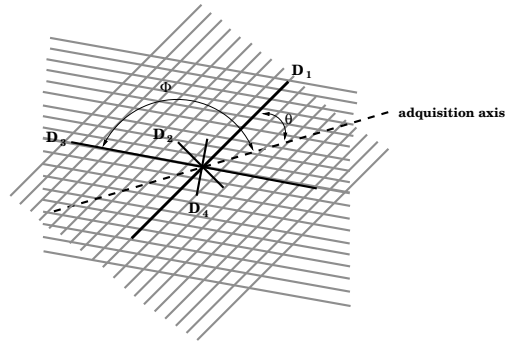


Figure 17. Angle θ of the first fiber (defined by the diffusion coefficients D_1 and D_2) with respect to the acquisition axis, and angle Φ of the second fiber (D_3 and D_4)

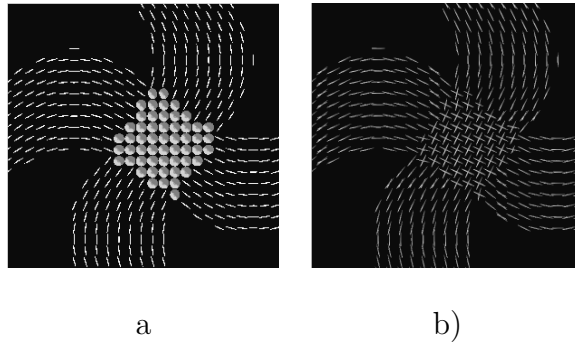


Figure 18. a) Synthetic DT-MRI computed with (22) and (23), for the case of 1 and 3 fibers respectively. b) Tensor basis decomposition.

The results of the validation procedure are following discussed. The input synthetic field is shown in Panel 18a, and the recovered multi-tensor field is shown in Panel 18b. The difference between the original diffusion orientation and the recovered PDD's has a peak error equal to 28.37 degrees and a mean error of 5.34 degrees (see panel 19a). The difference between the traces has a peak error equal to $0.04^{-3} \text{ mm}^2/\text{s}$ and a mean error equal to $0.009^{-3} \text{ mm}^2/\text{s}$ (see panel 19b). The peak angular errors are concentrated in a small regions at the border of the crossing zone. On the other hand, the negligible peak trace error is about 4% of the original trace. This error is more homogeneously distributed in the crossing zone. Note that the method reproduce the correct values at the high anisotropic regions.

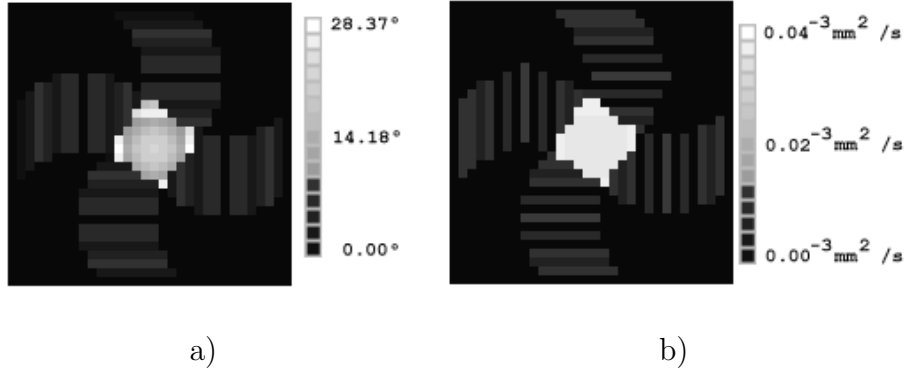


Figure 19. Error map of the recover multi-tensor field respect to the synthetic ground truth: a) angular and b)trace

5. Conclusions

We presented a method that improves the resolution of standard DT-MRI technique and allows one to reconstruct the intra-voxel information in fiber crossing and bifurcations. Therefore, we estimate the intra-voxel information from standard DT-MR images instead of compute it directly from raw data, as in (Tuch et al., 1999; Tuch et al., 2002; Tuch, 2002). In our method, the capture time for the DT-MR images is not modified but the computational time.

The presented method is based on the minimization of a cost function with quadratic potentials. So that, the minimization can be perform by gradient descent type methods or, as in our case, by a memory efficient Gauss-Seidel scheme. According to our experiments, the method is robust to the parameter set and the tensor basis selected.

The proposed multi-tensor restoration method can efficiently be used as a generic filtering method of tensor fields, as was demonstrated by experiments (see figure 15).

We presented a novel stochastic particle walk procedure based on Bayesian estimation theory and a second order Markov random process model. The procedure allow us to estimate the fiber pathways and therefore deduct the brain

connectivity. The stochastic movement of the particle allows one to explore possible bifurcations on fiber bundles.

Diffusion Tensor MRI (DT- MRI) is used for in vivo identification of fiber tracts in the human brain. However, interpretation of the DT-MRI is limited by the difficulty of post-mortem validations because of post-mortem delay and immersion fixation. So that, we validate our method with synthetic generated data with a model that consider the intra-voxel geometric structure. An opportunity for future research is the development of test database (phantoms) for evaluating the algorithms performance in the intra-voxel reconstruction problem.

Acknowledgments

We thank to J.C. Gee who gently provided us the DT-MRI data used in the experiments, to B.C. Vemuri and to the anonymous referees for their comments that improve the quality of the paper. The code for the method reported in (Pajevic et al., 2002) was obtained from the library Web page provided for the authors: <http://mscl.cit.nih.gov/spaj/dti/bcadt>. The authors were supported in part by CONACYT, Grant P40722Y1.

Appendix A. Noise Model

From (6), the noise model is given by $\bar{\eta}_r = \mathbf{D}_r - \sum_i^N \alpha_{ir} \bar{\mathbf{T}}_i$; where $\bar{\eta}$ is a residual tensor produced by the limited angular resolution of the tensor basis and noise. Given that the difference between two positive definite tensors is always a positive definite tensor, in this appendix, we show that if the residual produced by noise is of the form $\eta = R_\theta^T \mathbf{N} R_\theta$, then the Frobenius's norm is adequate for the data term in (9); where the diagonal matrix $\mathbf{N} = \text{diag}(n_1, n_2, n_3)$, with

$n_i \in \mathcal{N}(0, \sigma^2)$ are independent Gaussian variables and R_θ is an arbitrary rotation matrix. This is, the rotation angles, $\theta = [\theta_1, \theta_2, \theta_3]^T$, are uniformly distributed in the 3D space. Based on the noise model, the likelihood is given by (Geman and Geman, 1984): $P\left(\mathbf{D}_r \left| \sum_i^N \alpha_{ir} \bar{\mathbf{T}}_i \right.\right) = P(\eta_r)$. If we define $\mathbf{n} = [n_1, n_2, n_3]^T$, then $P(\eta_r) = \prod_i P(n_{ir}) = \frac{1}{\sqrt{2\pi\sigma}} \exp\left[-\frac{1}{\sigma^2} \mathbf{n}^T \mathbf{n}\right]$. Now, we have that $\mathbf{n}^T \mathbf{n} = n_1^2 + n_2^2 + n_3^2 = \|\mathbf{N}\|_F^2 = \|\eta_r\|_F^2$. Where $\|\cdot\|_F^2$ denotes the square Frobenius's norm. Note that last equality is based on the fact that the norm of the symmetric matrix η_r is invariant to rotations. So that, the likelihood is:

$$P\left(\mathbf{D}_r \left| \sum_i^N \alpha_{ir} \bar{\mathbf{T}}_i \right.\right) = \frac{1}{\sqrt{2\pi\sigma}} \exp\left[-\frac{1}{\sigma^2} \left\| \mathbf{D}_r - \sum_i^N \alpha_{ir} \bar{\mathbf{T}}_i \right\|_F^2\right]$$

and the negative log-likelihood corresponds to the Frobenius's norm.

References

- Basser, P. J., S. Pajevic, C. Pierpaoli, and A. Aldroubi: 2002, 'Fiber tract following in the human brain using DT-MRI data'. In: *IEICE Trans Inf Sys*, Vol. E85D. pp. 15–21.
- Basser, P. J., S. Pajevic, C. Pierpaoli, J. Duda, and A. Aldroubi: 1996, 'Microstructural and physiological features of tissues elucidated by quantitative-diffusion-tensor MRI'. *J. Magn. Reson.* **111**, 209–219.
- Basser, P. J., S. Pajevic, C. Pierpaoli, J. Duda, and A. Aldroubi: 2000, 'In Vivo Fiber Tractography Using DT-MRI Data'. *Magn. Reson. Med.* **44**, 625–632.
- Björnemo, M. and B. Anders: 2002, 'White Matter Fiber Tracking Using Diffusion Tensor MRI'. Reg nr: Liu-imt-ex-321, Linköping University.
- Buxton, R.: 2002, *Introduction to Functional Magnetic Resonance Imaging Principles and Techniques*. Cambridge University Press.
- Gee, J. C., D. C. Alexander, M. Rivera, and J. T. Duda: 2002, 'Non-rigid registration of diffusion Tensor MR Images'. In: I. Press (ed.): *IEEE International Symposium on Biomedical Imaging*. pp. 477–480.
- Geman, S. and D. Geman: 1984, 'Stochastic relaxation, Gibbs distribution and the Bayesian restoration of images'. *IEEE Transactions on Pattern Analysis and Machine Intelligence* **6**(6), 721–741.

- Hastie, T., R. Tibshirani, and J. Friedman: 2001, *The Elements of Statistical Learning: Data Mining, Inference, and Prediction*. Springer-Verlag.
- Lazar, M., D. M. Weinstein, J. S. Tsuruda, K. M. Hasan, K. Arfanakis, M. E. Meyerand, B. Badie, H. Rowley, V. Haughton, A. Field, and A. L. Alexander: 2003, 'White matter tractography using diffusion tensor deflection'. *Hum Brain Mapp* **18**(4), 306–21.
- Li, S. Z.: 2001, *Markov Random Field Modeling in Image Analysis*. Springer Verlag.
- Mardia, K. V.: 1972, *Statistics of Directional Data*. Academic Press.
- O'Donnell, L., S. Haker, and C. F. Westin.: 2002, 'New Approaches to Estimation of White Matter Connectivity in Diffusion Tensor MRI: PDE-Based and Geodesics in a Tensor-Warped Space'. In: *Fifth International Conference on Medical Image Computing and Computer-Assisted Intervention - MICCAI'02*.
- Pajevic, S., A. Aldroubi, , and P. J. Basserz: 2002, 'A Continuous Tensor Field Approximation of Discrete DT-MRI Data for Extracting Microstructural and Architectural Features of Tissue'. *Journal of Magnetic Resonance* **154**, 85100.
- Parker, G. J. M., C. A. M. Wheeler-Kingshott, and G. J. Barker: 2002, 'Estimating Distributed Anatomical Brain Connectivity Using Fast Marching Methods and Diffusion Tensor Imaging'. *IEEE Transactions on Medical Imaging* **21**(5), 505–512.
- Poldrack, R. A.: 2001, 'A structural basis for developmental dyslexia: Evidence from diffusion tensor imaging'. In: M. Wolf (ed.): *Dyslexia, Fluency, and the Brain*. pp. 213–233.
- Poupon, C., C. Clark, V. Frouin, J. Regis, I. Bloch, D. L. Bihan, and J. Mangin: 2000, 'Regularization of diffusionbased direction maps for the tracking of brain white matter fascicles'. *Neuroimage* **12**, 184–195.
- Ramirez-Manzanares, A. and M. Rivera: 2003, 'Brain Nerve Bundles Estimation by Restoring and Filtering Intra-Voxel Information in Diffusion Tensor MRI.'. In: *2nd IEEE Workshop on Variational, Geometric and Level Sets Methods in Computer Vision (VLSM 2003)*. Nice France, pp. 71–80.
- Ramirez-Manzanares, A., M. Rivera, B. Vemuri, and T. Mareci: 2004, 'Basis Functions for Estimating Intravoxel Structure in DW-MRI'. In: *To appear in Procc. IEEE Medical Imaging Conference 2004 (MIC 2004)*. Rome, Italy.
- Ruiz-Alzola, J., C. F. Westin, S. K. Warfield, A. Nabavi, and R. Kikinis: 2000, 'Nonrigid Registration of 3D Scalar, Vector and Tensor Medical Data'. In: *MICCAI 2000*. pp. 541–550.
- Tschumperlé, D. and R. Deriche: 2002, 'Orthonormal Vector Sets Regularization with PDE's and Applications'. In: *IJCV, International Journal of Computer Vision*.

- Tschumperlé, D. and R. Deriche: 2003a, ‘Tensor Field Visualization with PDEs and Application to DT-MRI Fiber Visualization’. In: *VLSM03*. pp. 255–262.
- Tschumperlé, D. and R. Deriche: 2003b, ‘Variational Frameworks for DT-MRI Estimation, Regularization and Visualization’. In: *Ninth IEEE International Conference on Computer Vision*, Vol. 1. pp. 116–121.
- Tuch, D. S.: 2002, ‘Diffusion MRI of complex tissue structure’. Ph.D. thesis, Harvard-MIT.
- Tuch, D. S., T. G. Reese, M. R. Wiegell, N. Makris, J. W. Belliveau, and V. J. Wedeen: 2002, ‘High angular resolution diffusion imaging reveals intravoxel white matter fiber heterogeneity’. *Magnetic Resonance in Medicine* **48**(4), 577.
- Tuch, D. S., R. M. Weisskoff, J. W. Belliveau, and V. J. Wedeen: 1999, ‘High angular resolution diffusion imaging of the human brain’. In: *Proc. 7th Annual Meeting of ISMRM*, Vol. 321.
- Vigueras, F.: 2001, ‘Filtrado y segmentacion de imagenes usando difusion anisotropica’. Master’s thesis, Centro de Investigacion en Matematicas (CIMAT).
- Wang, Z., B. C. Vemuri, Y. Chen, and T. Mareci: 2003, ‘A Constrained Variational Principle for Direct Estimation and Smoothing of the Diffusion Tensor Field from DWI’. In: *IPMI 2003*. pp. 660–671.
- Westin, C., S. Maier, H. Mamata, F. Jolesz, and R. Kikinis: 2002, ‘Processing and Visualization for Diffusion Tensor MRI’. *Medical Image Analysis* **6**(2), 93–108.
- Westin, C. F. and S. E. Maier: 2002, ‘A dual tensor basis solution to the stejskal-tanner equations for DTMRI’. In: *In Proceedings of International Society for Magnetic Resonance in Medicine*.
- Westin, C. F., S. E. Maier, B. Khidhir, P. Everett, F. A. Jolesz, and R. Kikinis: 1999, ‘Image Processing for Diffusion Tensor Magnetic Resonance Imaging’. In: C. A. Taylor C (ed.): *MICCAI 99*. pp. 441–452.
- Wiegell, M. R., M. Henrik, B. W. Larsson, and V. J. Wedeen: 2000, ‘Fiber Crossing in Human Brain Depicted with Diffusion Tensor MR Imaging.’. *Radiology* **217**, 897–903.
- Zhang, S., T. Curry, D. S. Morris, and D. H. Laidlaw: 2000, ‘Streamtubes and streamsurfaces for visualizing diffusion tensor MRI volume images.’. In: *Visualization ’00 Work in Progress*.
- Zhukov, L. and A. Barr: 2002, ‘Oriented Tensor Reconstruction: Tracing Neural Pathways from Diffusion Tensor MRI’. In: *Proceedings of IEEE Visualization 2002*. pp. 387–394.
- Zhukov, L., K. Museth, D. Breen, R. Whitaker, and A. Barr: 2003, ‘Level Set Modeling and Segmentation of DT-MRI Brain Data’. *Journal of Electronic Imaging* **12**(1), 125–133.